01 Jan 2014

Parametric Studies of the Thermal and Momentum Accommodation of Monoatomic and Diatomic Gases on Solid Surfaces

Zhi Liang

Pawel Keblinski

Recommended Citation

Z. Liang and P. Keblinski, "Parametric Studies of the Thermal and Momentum Accommodation of Monoatomic and Diatomic Gases on Solid Surfaces," *International Journal of Heat and Mass Transfer*, vol. 78, pp. 161 - 169, Elsevier, Jan 2014.
The definitive version is available at https://doi.org/10.1016/j.ijheatmasstransfer.2014.06.038

International Journal of Heat and Mass Transfer 78 (2014) 161–169

Contents lists available at ScienceDirect

International Journal of Heat and Mass Transfer

journal homepage: www.elsevier.com/locate/ijhmt

Parametric studies of the thermal and momentum accommodation of monoatomic and diatomic gases on solid surfaces

Zhi Liang [a,*], Pawel Keblinski [a,b,*]

[a] Rensselaer Nanotechnology Center, Rensselaer Polytechnic Institute, Troy, NY 12180, USA
[b] Department of Materials Science and Engineering, Rensselaer Polytechnic Institute, Troy, NY 12180, USA

ARTICLE INFO

Article history:
Received 9 March 2014
Received in revised form 9 June 2014
Accepted 12 June 2014
Available online 17 July 2014

Keywords:
Thermal accommodation coefficient
Momentum accommodation coefficient
Molecular dynamics

ABSTRACT

The thermal accommodation coefficient (TAC) and the momentum accommodation coefficient (MAC) are the two fundamental parameters quantifying the solid–gas energy and momentum exchange efficiencies. We use molecular dynamics (MD) simulations to study the effect of individual interfacial parameters including, (i) solid–gas interaction strength, (ii) gas–solid atomic mass ratio, (iii) solid elastic stiffness, and (iv) temperature, on TAC and MAC at solid surfaces in contact with monoatomic and diatomic gases. In addition to offering a fundamental understanding on how these individual parameters affect the nature of gas–solid collisions, we provide an extensive database for the TAC and MAC. We also study the effect of surface functionalization with molecular monolayers on the energy and momentum transfer at the interface. These results are useful in developing interfaces with enhanced heat transfer under various operation conditions.

1. Introduction

Convective heat transfer in rarefied gases is of great importance to the thermal management of microelectronic devices [1–3], microelectromechanical systems (MEMS) based devices [4], and aircraft flying at high altitudes [5,6]. The degree of rarefication of a gas can be described by the Knudsen number $Kn = \lambda/L$, where λ is the mean free path of gas molecules and L is a characteristic dimension. A gas is regarded as rarefied if $Kn > 0.01$ [6], which means λ is not negligible compared to L. This happens in two ways, either because of a large λ, or due to a very small L. The first case occurs when gas pressure is very low, for example air at very high altitudes. The second case occurs when the dimensions of objects are very small, for example micro/nano-channels in cooling element of microelectronic devices or MEMS based devices. In both cases, the number of collisions between the gas molecules and the wall is larger than the number of collisions between the molecules in vicinity of the solid wall. Accordingly, the energy and momentum transfer at solid–gas interfaces could strongly affect the overall heat transfer efficiency.

In order to investigate the heat transfer to a body in a rarefied gas, the well-established continuum theories must be modified to account for the velocity slip and temperature jump at the solid wall [4–6]. According to the gas kinetic theory [7,8], the velocity-slip and temperature-jump boundary conditions can be incorporated by introducing two parameters called momentum accommodation coefficient (MAC), defined as the fraction of gas molecules reflected diffusely from the solid surface, and thermal accommodation coefficient (TAC), defined as the fraction of gas molecules incident on the surface scattered in thermal equilibrium with the surface.

Despite the fact that the subjects of the TAC and MAC have over a century-long history of investigation, presently no quantitative theory exists and there are only semi-quantitative or empirical formulas available to fit experimental data [9]. These formulas have limited applicability to a wide range of gas–solid interfaces and temperatures. Moreover, the role of individual parameters is often difficult to determine in experiments [6]. To understand and quantify the role of individual interfacial parameters and to determine how these parameters affect the nature of gas–solid collisions and the value of the TAC and MAC, we resort to molecular dynamics (MD) simulations and a suite of molecular-level thermal characterization techniques.

Molecular simulations are uniquely positioned to explore the mechanism behind the energy and momentum transport at solid–gas interfaces. In the past decade, the MD simulation has been utilized to study the TAC and MAC of noble gases on various solid surfaces [1,2,10–12]. However, each of these work only investigated one or two factors that influence TAC or MAC.

* Corresponding authors. Tel.: +1 5185451584.
E-mail addresses: liangz3@rpi.edu (Z. Liang), keplip@rpi.edu (P. Keblinski).

http://dx.doi.org/10.1016/j.ijheatmasstransfer.2014.06.038
0017-9310/

Moreover, a systematic study of effects of various parameters on the TAC and MAC of diatomic or polyatomic gases is not available. In this work, we carry out a systematic study of the effects of various parameters of importance, including the solid–gas interaction strength, the gas–solid mass ratio, and the temperature and elastic modulus of solid on the TAC and MAC. In addition to study the accommodation coefficients of monoatomic gases on solid surfaces, we also investigate the TAC and MAC of diatomic gases and the effect of surface modification such as the functionalization of the solid with self-assembled monolayers (SAMs) on thermal and momentum accommodation of various gases. Through the extensive MD simulations, we will generate a database for TAC and MAC and provide a fundamental understanding of the nature of thermal and momentum accommodation for monoatomic and diatomic molecules.

2. Determination of TAC and MAC using MD simulations

2.1. Theory

In the case of monoatomic gases TAC is defined by [9]

$$\alpha_T = (T_r - T_i)/(T_s - T_i) \tag{1}$$

where T_i and T_r are the temperatures of incident and reflected gas atoms, respectively, and T_s is the solid surface temperature. $\alpha_T = 1$ means there is a complete thermal equilibration of the incident gas stream with the solid. In the case of diatomic gases, the TAC can be also calculated by Eq. (1), if the diatomic molecule can be approximated as a classical rigid rotor. For diatomic gases, we can further calculate the translational and rotational temperatures of gas molecules, thus obtain the TACs for translational and rotational molecular motions.

In the temperature jump regime ($0.01 < Kn < 0.1$), TAC relates to the solid–gas interfacial thermal conductance G_K by [8]

$$G_K = f k_B N \alpha_T/(2 - \alpha_T) \tag{2}$$

where $f = 4$ for a monoatomic gas and $f = 6$ for a diatomic gas, k_B is the Boltzmann constant, and N is collision rate per unit area. The collision rate is a function of pressure, P, temperature, T, and the atomic mass m, and it is given by [8]

$$N = P/\sqrt{2\pi m k_B T} \tag{3}$$

The interfacial thermal conductance can be readily obtained from non-equilibrium MD (NEMD) simulations using

$$G_K = q/\Delta T \tag{4}$$

where q is the heat flux across the solid–gas interface, and ΔT is a temperature jump at the solid–gas interface. Hence, the relation between G_K and α_T given by Eq. (2) can be used to verify the consistency of the TAC calculated directly by Eq. (1) and via Eq. (2).

Similar to Eq. (1), the equation to calculate tangential-MAC is [13]

$$\alpha_v = (v_{x,r} - v_{x,i})/(v_{x,s} - v_{x,i}) \tag{5}$$

where $v_{x,i}$ and $v_{x,r}$ are the tangential velocities of incident and reflected gas molecules, respectively, and $v_{x,s}$ is the tangential velocity of solid surface. $\alpha_v = 1$ means all gas molecules are diffusely scattered by the surface. If $v_{x,s} = 0$ which is the case in our MD simulation, Eq. (5) can be simplified to Eq. (6).

$$\alpha_v = 1 - v_{x,r}/v_{x,i} \tag{6}$$

According to Eq. (6) $v_{x,r}$ is linearly proportional to $v_{x,i}$ if the macroscopic velocity of the solid is zero. This relation is utilized in our MD simulations to calculate the tangential-MAC.

2.2. MD model

The model system consists of a solid Au slab in contact with Ar or N_2 gas, as depicted in Fig. 1(a). The Au slab is formed by a nine layers of FCC (1 1 1) planes of solid Au with a cross section area of 5.2 nm by 5.0 nm. The length of the gas region, L, is 102 nm. Periodic boundary conditions are applied in all three directions. The embedded-atom-method (EAM) potential [14] is used for Au–Au interactions. The Lennard-Jones (LJ) 12-6 potential, with parameters $\sigma = 3.41$ Å and $\varepsilon = 10.3$ meV [15], is employed for Ar–Ar interactions. The N_2 molecule with a bond length of 1.10 Å [16] is considered as a rigid rotor in the MD simulation. The LJ potential, with parameters $\sigma = 3.31$ Å and $\varepsilon = 3.21$ meV [17], is employed for N–N interactions between molecules.

In the case of Au surfaces functionalized with SAMs, 120 1-octanethiolate [-S-$(CH_2)_7$-CH_3] chains are covalently bonded to Au surface and form a two-dimensional triangular lattice with a surface density of 1/(21.6 Å^2). The interatomic interactions for SAM molecules are described by the Hautman–Klein united atom (UA) model [18], which treats the hydrocarbon groups as single interaction sites. LJ potentials are used for non-bonded interactions in SAM molecules in the UA model. The Koike–Yoneya bond stretching potential [19] is included in the UA potential to take into account the C–C and C–S bond stretching motions. The Au–S interactions are modeled by the Morse potential $V(r) = D(e^{-2a(r-r_e)} - 2e^{-a(r-r_e)})$ with parameters $r_e = 2.65$ Å, $a = 1.47$ Å^{-1} and $D = 0.15$ eV [1,20]. LJ potentials for interactions between Au and other atoms in SAMs are taken from the universal force field (UFF) [21].

The solid–gas interactions are all described by the LJ potential with parameters calculated by the Lorentz–Berthelot mixing rule.

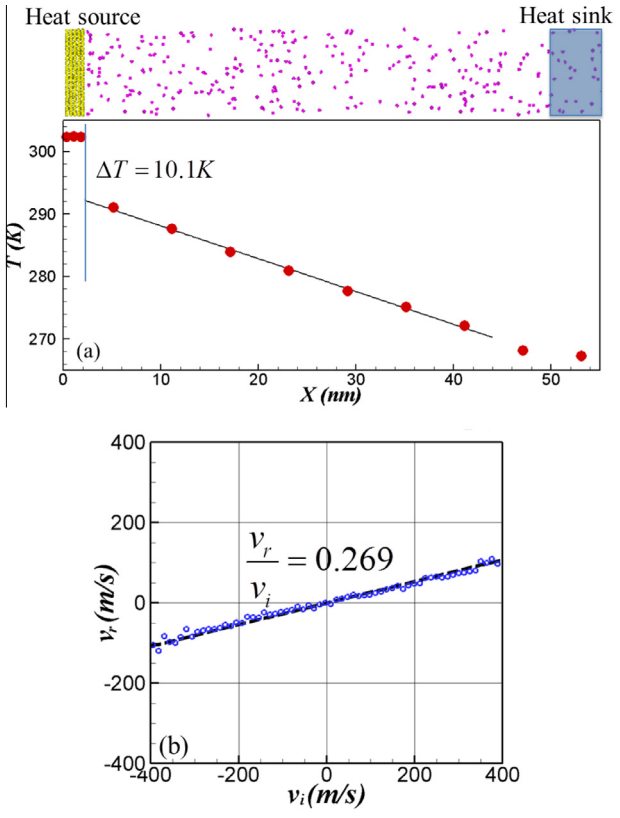

Fig. 1. (a) A snapshot of solid–gas system and the steady state temperature profile. Due to the symmetry of the system, only half of the simulation box is shown. (b) The reflected tangential velocity as a function of the incident tangential velocity. The dashed line is a linear fit to the simulation data.

The cutoff distance for all LJ interactions is 11 Å in the simulation. The standard ε_{sf} for Ar–CH_3 interaction is 8.85 meV, which is about twice of ε_{sf} for N–CH_3 interaction. In studying the effect of surface modification, we will compare the TACs and MACs on a SAM surface and on a bare Au surface with the same solid–gas interaction strength. Hence, the standard ε_{sf} for the Ar–CH_3 interaction and for the N–CH_3 interaction is also used for the Ar–Au interaction and N–Au interaction, respectively, in the reference system.

The total number of gas molecules in the model system is determined by PV/k_BT according to the ideal gas law, where V is the volume of the gas region. For reference systems with the standard ε_{sf}, there are very few gas molecules adsorbed on the solid surface at room temperature [1,2]. For systems with higher ε_{sf}, however, a considerable number of gas atoms are bonded to the surface; thus we increase the total number of gas molecules to maintain the gas at the desired pressure.

2.3. Simulation details

All MD simulations, except for those studying the temperature effect, are performed at 300 K, 15 bar for monoatomic gases, and 300 K, 10 bar for diatomic gases. A relatively higher pressure is used in the simulation so as to get a better statistics within finite simulation time. The energy and momentum exchange coefficients do not depend significantly on pressure when the gas adsorption is small or well established. However, in the transitional region the pressure will affect the adsorption coverage, thus will change the accommodation coefficients [11]. The mean free path, λ, of gas molecules is about 5 nm [8] in both cases. Consequently, $Kn = \lambda/L$ is about 0.05, which belongs to the temperature jump regime in gas dynamics problems.

If the model system only contains Au and Ar, a velocity Verlet scheme is used for the integration of the equations of motions [22]. If the system contains N_2, a leapfrog formulation for quaternions proposed by Omelyan [23] is used for the integration of the equations of rotational motions. In all these simulations, a single time step, of 4 fs is used. When Au surfaces are functionalized with SAMs, a velocity Verlet scheme with multiple time steps is used for the integration of the equations of motions [22]. A time step size of 1 fs is used for bond stretching; 2 fs is used for bond bending, torsion, and Au–S interactions; 4 fs is used for all other interactions. For all systems, a constant NVT simulation is firstly carried out for 2 ns. The Berendsen et al.'s algorithm [24], with a time constant of 2 ps, is used to equilibrate the system to the preset temperature.

In the subsequent production runs, the global thermostat is eliminated, and a heat flux of 16 MW/m^2 is applied to the system via a heat source-sink method. The gas region is divided evenly into 17 bins. The middle 3 bins in the gas phase are set as the heat sink region, and the Au slab is set as the heat source region. Energy is added to the heat source at a constant rate of 0.415 nW; it is removed at the same rate in the heat sink by velocity rescaling at each time step [25]. For the N_2 gas in the heat sink, 60% of the energy removal is from reduction in translational kinetic energy and the rest 40% is from rotational kinetic energy since the diatomic molecule has 3 degrees of freedom in translational motions and 2 degrees of freedom in rotational motions. Each heat source-sink simulation run is first carried out for 12 ns to allow the system to reach a steady state, and then, for an additional 40 ns for data collection and averaging.

To calculate the TACs and MACs using Eq. (1) and (6), we set an imaginary plane 11 Å (cutoff distance) away from the solid surface. The small distance between the plane and surface ensures that the collisions between gas atoms moving from the plane to the solid surface and back are rare by comparison with the collisions with the solid. The incident (or reflected) gas molecules pass through the imaginary plane indicating the start (or finish) of the energy and momentum exchange process. The temperature of incident (or reflected) gas molecules is obtained by dividing the average kinetic energy of the incident (or reflected) molecules by $2k_B$ for monoatomic gases, and by $3k_B$ for diatomic gases [8]. For diatomic gases, we further divide the kinetic energy into translational and rotational kinetic energies, and thus calculate the translational and rotational components of the TACs.

To calculate MACs, we monitor the tangential velocity of incident molecules ranging from −400 to 400 m/s. Out of this range, the statistics is poor within the finite simulation length. For each incident tangential velocity $v_{x,i}$, we calculate the average reflected tangential velocity $v_{x,r}$. To get good statistics, $v_{x,i}$'s are divided into bins with the width of 6 m/s. The slope of linear fit of $v_{x,r}$ vs. $v_{x,i}$ is used to determine MAC based on Eq. (6). The uncertainties are determined from the analysis of eight independent simulation runs.

3. Simulation results

3.1. TAC and MAC in the reference system

3.1.1. Monoatomic gas reference system

The reference system consists of an Au slab in contact with Ar gas at 300 K and 15 bar. The standard Ar–CH_3 interaction strength ε_{sf} = 8.85 meV corresponding to $0.34k_BT$ is used for the Ar–Au interaction in the simulation. The steady state temperature profile is shown in Fig. 1(a). Using the temperature drop at the solid–gas interface, we obtain $G_K = 0.79 \pm 0.04$ MW/m^2 K which, according to Eq. (2), corresponds to $\alpha_T \approx 0.56 \pm 0.02$. From the NEMD simulation, we also obtain $T_i = 287.0$ K, $T_r = 295.5$ K, and $T_s = 302.4$ K. According to the definition of TAC in Eq. (1), $\alpha_T = 0.55 \pm 0.01$. The consistency between the α_T's from the two calculation methods indicates the distance of the imaginary plane from the solid surface is appropriate in our calculation. Fig. 1(b) shows the reflected tangential velocity $v_{x,r}$ as a function of the incident tangential velocity $v_{x,i}$. It is evident that the data can be fitted by a linear function with a slope of 0.269 very well. Using Eq. (6) we obtain $\alpha_v = 0.73 \pm 0.01$.

3.1.2. Diatomic gas reference system

A similar procedure to that described above is used to determine the TAC and MAC of N_2 gas on a Au slab at 300 K and 10 bar. For the reference system with N_2 gas, we set $\varepsilon_{N-Au}/k_BT = 0.171$, which is half of the Ar–Au interaction strength, although it corresponds to the same molecular adsorption energy since there are two atoms in a N_2 molecule. From the temperature profile we obtain $G_K \approx 0.52 \pm 0.03$ MW/m^2K, which corresponds to $\alpha_T = 0.38 \pm 0.02$. By directly calculating T_i, T_r, and T_s at the imaginary plane, we obtain $\alpha_T = 0.36 \pm 0.02$. The two α_T's are again in good agreement. Furthermore, we find the TAC of translational motion $\alpha_{tr} = 0.40 \pm 0.03$ and the TAC of rotational motion $\alpha_{rot} = 0.29 \pm 0.03$. The result shows the rotational motion is more difficult to thermalize with the solid surface in the reference system. Finally, the linear fit of $v_{x,r}$ vs. $v_{x,i}$ gives α_v of N_2 is 0.57 ± 0.01.

A similar method is employed to calculate the TACs and MACs in the following parametric study. The TAC results in the following figures are all calculated from Eq. (1).

3.2. The mass effect on the TAC and MAC of a monoatomic gas

The mass effect on the TAC has been studied theoretically by the hard-sphere collision model which predicts $\alpha_T = 2.4\mu/(1+\mu)^2$ where μ is the ratio of gas to solid atom mass [8]. According to this model, the maximum α_T is obtained when the mass of gas atom is

the same as that of solid atom. However, this model misses a number of important factors, such as the interaction strength between solid atoms and solid–gas interaction strength [2].

3.2.1. Effect of mass of gas atoms

To study the mass effect, we artificially vary the mass of Ar to the mass of He, Ne, Kr, and Xe, while keeping all other parameters the same as those in the reference system. Accordingly, the mass ratio m_g/m_{Au} varies from 0.02 to 0.67. When the mass ratio is less than 1, the hard-sphere model predicts that the TAC increases monotonically with the mass ratio. The MD simulation results of the TAC at $\varepsilon_{sf}/k_BT = 0.342$ are shown in Fig. 2(a). Evidently, the TACs from MD simulations are larger than those from the hard-sphere model, though the general trend of the mass-ratio dependence is similar.

The gas–surface collisions can be evaluated based on two distinct dynamics, direct collision dynamics and trapping–desorption dynamics [26]. The hard-sphere collisions can only account for direct collisions. The trapping–desorption dynamics becomes more important as ε_{sf} gets larger [1,2]. To evaluate the influence of ε_{sf} on the simulation results, similar MD simulations are performed with $\varepsilon_{sf}/k_BT = 0.171$ and $\varepsilon_{sf}/k_BT = 1.05$. In the former case, the gas–surface collisions are dominated by direct collision dynamics. In the latter case, the trapping–desorption dynamics dominates [1,2]. It is shown in Fig. 2(a) that even with a very small ε_{sf}, the MD simulation results have only moderate agreement with the theoretical

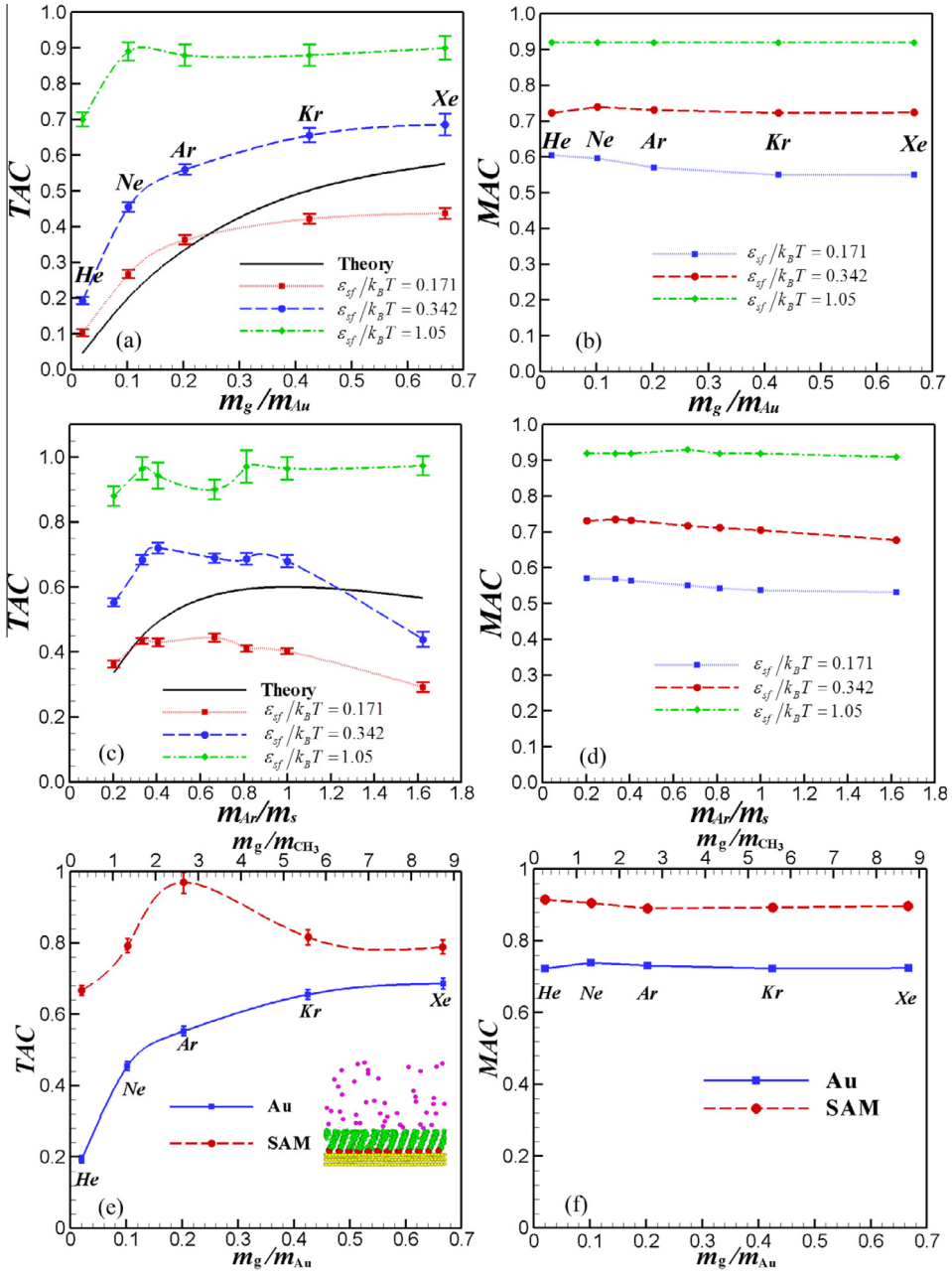

Fig. 2. The TAC and MAC as a function of the gas–solid mass ratio at 300 K. (a) The TAC on a bare Au surface. The mass of solid atom is fixed. The mass of gas atom varies from the mass of He to the mass of Xe. The solid line represents the prediction from the hard-sphere model. (b) Same as (a) but for the MAC. (c) The TAC of Ar on a bare solid surface. The mass of gas atom is fixed. The mass of solid atoms varies from 197 (m_{Au}) to 24.6. The black solid line represents the prediction of the hard-sphere model. (d) Same as (c) but for the MAC. (e) The TAC on a bare Au surface and a SAM surface. The inset shows a monoatomic gas snapshot in the vicinity of an Au surface functionalized with SAMs. The mass of the solid atom and SAM molecules are fixed. The mass of the gas atom varies from the mass of He to mass of Xe. (f) Same as (e) but for the MAC. The solid and dashed lines connecting simulation data are used to guide the eye (same for the following figures).

values if the mass ratio is less than 0.4. When the trapping–desorption dynamics dominates ($\varepsilon_{sf}/k_BT = 1.05$), the TACs are essentially mass independent and close to the theoretical maximum ($\alpha_T = 1$) if the mass ratio is greater than 0.1. A relatively small TAC for $m_{He}/m_{Au} \approx 0.02$ is mainly due to very large mass mismatch between solid and gas atoms, which leads to a highly inefficient energy transfer.

The mass effect on the MAC is shown in Fig. 2(b). Similar to the TAC, we find the MAC increases with ε_{sf}. However, the MAC is essentially mass independent for a given ε_{sf}. The result indicates that the mass ratio is not a critical factor affecting the MAC.

3.2.2. Effect of mass of solid atoms

To further study the mass effect, we artificially tune the mass of Au from 197 to 24.6 and calculate the TAC and MAC of Ar on the surface of solids with various masses. In this case, the mass ratio m_{Ar}/m_s varies from 0.20 to 1.63. The MD simulation results of the TAC are shown in Fig. 2(c). Similar to what we found in Fig. 2(a), the TAC from the hard-sphere model only agrees with the MD simulation results when $\varepsilon_{sf}/k_BT = 0.171$ and mass ratio is less than 0.4. The result indicates that the hard-sphere model can predict reasonable TACs only in the case of light gas atoms striking heavy surface atoms and, as discussed above, when the solid–gas interactions are weak.

The MD simulation results in Fig. 2(c) show that for a given ε_{sf} the TAC is essentially a constant for a mass ratio between 0.3 and 1. For a mass ratio less than 0.3, the inefficient energy transfer between highly mass-mismatched gas and solid atoms results in a smaller TAC. If the gas atom is heavier than the solid atom, a decrease in the TAC is found for $\varepsilon_{sf}/k_BT = 0.171$ and $\varepsilon_{sf}/k_BT = 0.342$. For $\varepsilon_{sf}/k_BT = 1.05$, however, the mass effect on the TAC is weak because the gas–surface collisions are dominated by trapping–desorption dynamics.

The mass-ratio dependence of MAC shown in Fig. 2(d) is similar to that in Fig. 2(b). MAC increases with ε_{sf}, but is essentially independent of mass ratio.

3.2.3. The mass effect on a SAM surface

In our previous work [1], we have shown that the TAC of Ar on a solid surface can be significantly enhanced by functionalizing the solid surface with SAMs. In this work, we study the mass effect on the TAC of monoatomic gases on a SAM surface. Again, we artificially vary the mass of Ar to the mass of He, Ne, Kr, and Xe while keep all other parameters unchanged. The mass of surface atom (a pseudo-atom in the UA model) of the SAM molecule equals the mass of CH_3. Therefore, the mass ratio m_g/m_{CH3} varies from 0.26 to 8.7 as shown in the top x-axis of Fig. 2(e). As a comparison, we put MD simulation results of the TAC on a SAM surface and on a bare Au surface together in Fig. 2(e). The standard solid–gas interaction strength $\varepsilon_{sf} = 8.85$ meV is used in all these MD simulations. It is shown in Fig. 2(e) that the TAC on a SAM surface is always larger than that on a bare Au surface. This result is consistent with findings in molecular beam experiments [26–28] where a highly efficient solid–gas energy exchange was observed when the solid surface is modified with SAMs. This is mainly because the SAM surface is much softer and more corrugated than the bare Au surface [1]. It is interesting to see that the TAC on a SAM surface has a maximum at mass ratio of about 2.6. The gas atoms collide directly with the surface atom of SAM molecules. However, the surface atom is tightly bonded to its first and second nearest pseudo-atoms in the molecular chain due to the strong stretching and bending strength in the SAM molecule. The third nearest pseudo-atom is subject to much weaker torsion strength. Hence, it is more appropriate to consider the mass of the surface atom in the SAM molecule as the sum of the mass of the three pseudo-atoms, which are closest to the surface. In this case, the m_s of the SAM surface is about 43 and the gas–solid mass ratio is about 0.93. This indicates that the maximum TAC on the SAM surface is due to the almost perfect mass matching between the solid and gas atoms.

The MAC of monoatomic gases on a SAM surface and a bare Au surface is shown in Fig. 2(f). Again, it is shown that the MAC is independent of mass ratio. Since the same solid–gas interaction strength is used in all these simulations, the larger MAC on the SAM surface is not due to the higher ε_{sf}. The SAM surface is much softer and more corrugated than the bare Au surface. A softer surface can increase the solid–gas interaction time [1], which leads to a more efficient exchange of momentum upon collision. A corrugated surface can scatter the gas molecules more diffusely than the smooth Au surface. Both effects result in enhancement in the MAC.

3.3. The temperature effect on the TAC and MAC of a monoatomic gas

To study the temperature effect, we vary the temperature of the reference system from 150 to 600 K. Accordingly, ε_{sf}/k_BT decreases from 0.684 to 0.171. The mean free path of gas molecules mainly depends on gas density [29]. Therefore, the gases are maintained at the same density rather than the same pressure at different temperatures, such that the position of the imaginary plane is always appropriate for the TAC and MAC calculations. The time step size

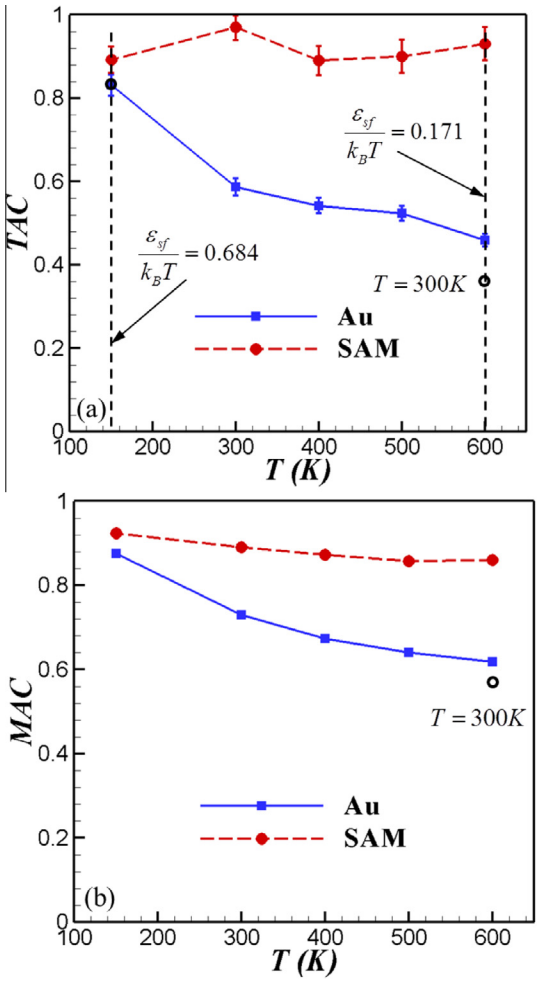

Fig. 3. (a) The TAC, and (b) the MAC of Ar on a bare Au surface and a SAM surface as a function of temperature. The open circles are the TAC and MAC for $\varepsilon_{sf}/k_BT = 0.171$ and $T = 300$ K.

is reduced at high temperatures to ensure good energy conservation.

The TACs of Ar on a bare Au surface and a SAM surface as a function of temperature are shown in Fig. 3(a). It is seen that the TAC of Ar on a SAM surface is close to unity and essentially temperature independent, while the TAC of Ar on a bare Au surface decreases with temperature. This result is consistent with TAC measurements in experiments [30] where TAC of Ar on a Pt surface was found decreasing with increasing temperature. This result can be also compared to our previous MD simulations for the same systems [1] in which we kept the temperature constant at 300 K while varying ε_{sf} to different values. We find the dependence of the TAC on ε_{sf}/k_BT in our current and previous simulations are almost the same. The result indicates that the increase of temperature is almost equivalent to decrease of ε_{sf} with the same ratio.

However, the increase of temperature can also lead to a slightly more corrugated solid surface due to more intense thermal motions of solid atoms. A corrugated surface is beneficial to energy and momentum exchange between solid and gas. As shown in Fig. 3(a), the TAC at 600 K with $\varepsilon_{sf}/k_BT = 0.171$ is larger than that at 300 K with the same ε_{sf}/k_BT. Hence, the increase of temperature has two effects on the TAC. On one hand, a higher temperature means a higher kinetic energy of gas molecules such that gas molecules are more difficult to adsorb on the surface. This effect reduces the TAC. On the other hand, higher temperature results in larger thermal roughness on the solid surface, which increases TAC.

In Fig. 3(b), we show temperature dependence of the MAC. On a SAM surface, MACs are around 0.9 in all cases. The temperature effect on the MAC is weak. On a bare Au surface, the increase of temperature is roughly equivalent to the decrease of ε_{sf} and results in a decrease in the MAC. It is shown in Fig. 3(b) that the MAC at 600 K with $\varepsilon_{sf}/k_BT = 0.171$ is larger than that at 300 K with the same ε_{sf}/k_BT. The difference can be also attributed to a more corrugated surface at the high temperature.

3.4. The effect of solid elasticity on TAC and MAC of a monoatomic gas

The elastic modulus (Young's modulus), E, of solid Au is about 78 GPa [31]. Many other materials such as Pt and W are much stiffer than Au. To study the effect of solid elasticity, we tune the prefactor in the EAM potential from 0.3 to 5. Since the elastic modulus is proportional to the prefactor, E of the solid varies from 23.4 to 390 GPa. The time step size is reduced accordingly as E gets bigger. All other parameters are the same as those in the reference system.

As shown in Fig. 4(a), the TAC decreases almost linearly with increasing E. When E is small, the gas atoms collide essentially with individual solid atoms since the solid atoms are weakly connected to each other. As E gets greater, solid atoms are more tightly bonded to each other. In this case, the gas atoms collide with multiple atoms, i.e., effectively a heavier solid atom, which results in larger mass mismatch and a smaller TAC. In the limit of an

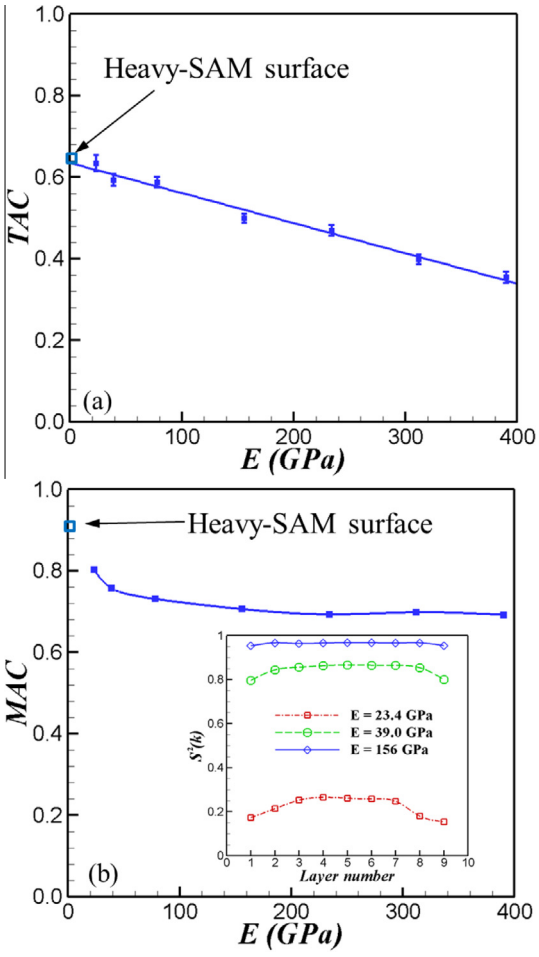

Fig. 4. The TAC and MAC of Ar on a bare solid surface as a function of elastic modulus. (a) The TAC vs. elastic modulus. The open square symbol represents the TAC of Ar on a heavy-SAM surface. (b) The MAC vs. elastic modulus. The open square symbol represents the MAC of Ar on a heavy-SAM surface. The inset shows the square of the planar structure factor for several elastic moduli.

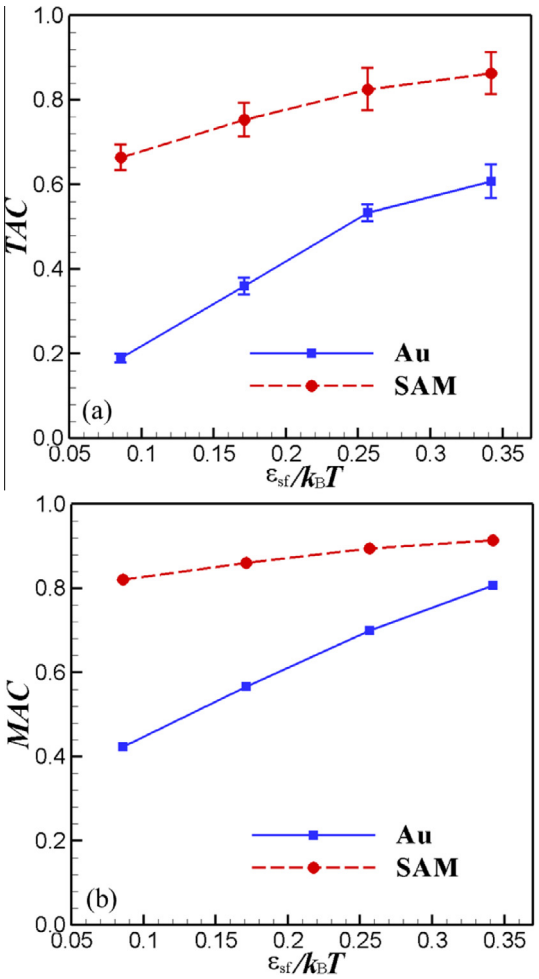

Fig. 5. (a) The TAC and (b) the MAC of N_2 on a bare Au and a SAM surface as a function of solid–gas interaction strength.

extremely large E, the gas atoms collide with a rigid elastic medium, and the TAC → 0. Obviously, the linear relation between the TAC and E shown in Fig. 4(a) cannot be extended to the region of much higher E since the TAC cannot be negative.

In Fig. 4(a), we also show the TAC on a heavy-SAM surface in which we artificially change the mass of pseudo-atom CH_3 to the mass of Au. By calculating the strain in SAM under a stress of ±0.025 GPa, we obtain the E of the SAM surface to be about 3.4 GPa. Therefore, a heavy-SAM surface mimics a bare Au surface with an $E \to 0$. It is seen in Fig. 4(a) that the TAC on a heavy-SAM surface is consistent with the linear extrapolation of TACs on a bare Au surface at $E = 0$. Hence, the linear relation between the TAC and E appears to be valid in the limit of $E \to 0$.

The dependence of the MAC on E is shown in Fig. 4(b). If E is greater than 50 GPa, the MACs are all round 0.7. Although there is almost no energy exchange between solid and gas at very high E, the atomic-scale surface roughness could lead to at least partially diffuse scattering of small gas molecules. Hence, the MAC does not approach zero at very high E. However, the MAC exhibits a fast increase with decreasing E if E is less than 50 GPa. Moreover, the MAC on the heavy-SAM surface is about 0.91, which is much higher than that on a bare Au surface. To understand the strong dependence of the MAC on E in the small E region, we calculate the square of planar structure factor, $S(k)$, in each atomic layer of the Au slab [32].

$$S^2(\vec{K}) = \left[\frac{1}{n}\sum_{i=1}^{n}\cos(\vec{K}\cdot\vec{r}_i)\right]^2 + \left[\frac{1}{n}\sum_{i=1}^{n}\sin(\vec{K}\cdot\vec{r}_i)\right]^2 \quad (7)$$

where r_i is the position of atom i in the given layer of Au slab, n is the number of atoms in the layer, and k is the reciprocal lattice vector of the (1 1 1) plane. $S^2(k)$ is unity in a perfect crystal structure and near zero in the liquid or amorphous states.

It is shown in the inset of Fig. 4(b) that $S^2(k)$ decreases as E gets smaller. A significant drop of $S^2(k)$ is observed when E is reduced from 39.0 to 23.4 GPa. This behavior is related to the decreased melting temperature T_m in solid. The T_m of Au with standard EAM potential is 1281 K [33]. Since the T_m is proportional to the prefactor. For E = 23.4 GPa (prefactor = 0.3) the T_m drops to 384 K which is close to the simulation temperature 300 K. It is reasonable to see the structure of solid becomes liquid-like especially at the surface region when the temperature is close to T_m. The liquid-like structure is responsible for the enhanced MAC for solids with a small E.

3.5. The effect of solid–gas interaction strength on the TAC and MAC of a diatomic gas

The solid–gas interaction strength ε_{sf}/k_BT is tuned from 0.0855 to 0.342 for N_2 on a bare Au surface and N_2 on a SAM surface at 300 K and 10 bar. The number of N_2 molecules is increased at a high ε_{sf} to maintain the gas at 10 bar. As shown in Fig. 5(a), the TAC on a bare Au surface increases with ε_{sf}. When the Au surface is functionalized with SAMs, the TAC is significantly enhanced and also increases with ε_{sf}. These results are similar to what we found on the TAC of Ar on a bare Au surface and a SAM surface [1]. The difference is the TAC of Ar on a SAM surface is essentially

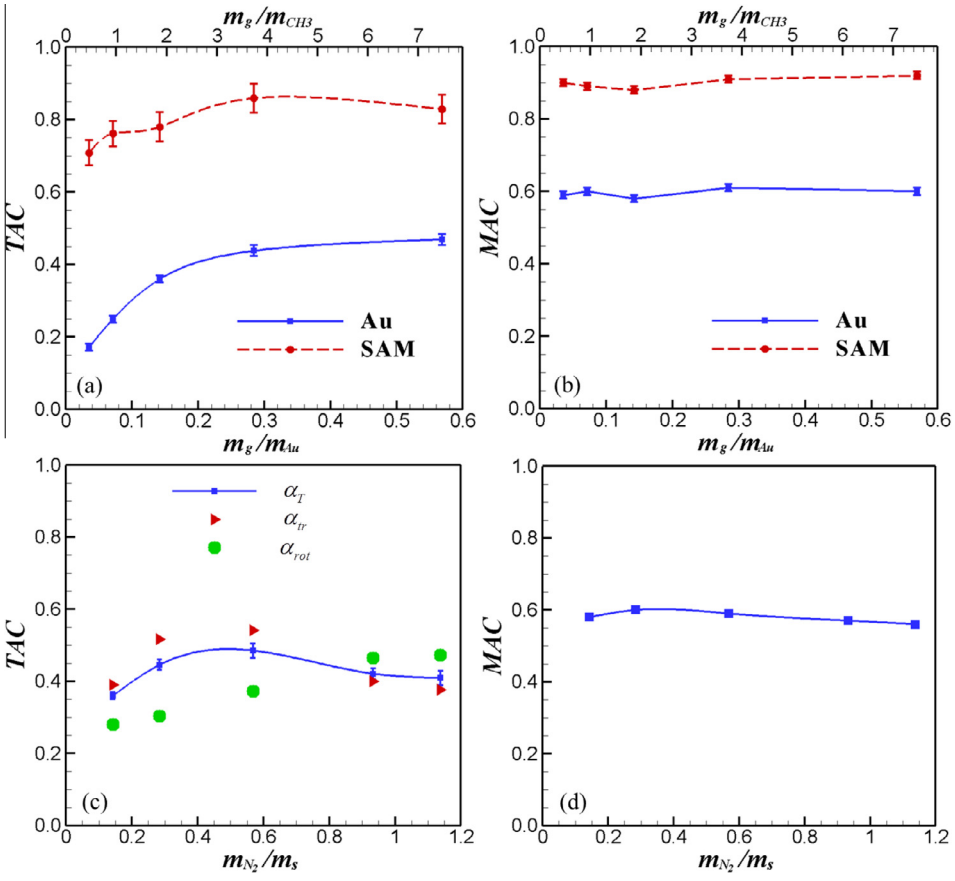

Fig. 6. The TAC and MAC of a diatomic gas as a function of gas–solid mass ratio at 300 K. (a) The TAC and (b) the MAC on a bare Au surface and a SAM surface. The mass of solid atoms is fixed. The mass of N is varied from 3.5 to 56. (c) The TAC and (d) the MAC on a bare solid surface. The mass of N is fixed at 14. The mass of Au is varied from 197 to 24.6.

independent of ε_{sf}. This difference may come from the relatively lower α_{rot} of N_2. For instance, with $\varepsilon_{sf}/k_BT = 0.171$ α_{tr} of N_2 increases from 0.40 (on the bare Au surface) to 0.83 (on the SAM surface) and α_{rot} increases from 0.29 to 0.59. The result shows the rotational motion of N_2 is also difficult to fully thermalize with the soft SAM surface.

Similar ε_{sf} dependence of the MAC is found in Fig. 5(b). On a SAM surface, however, the ε_{sf} dependence of the MAC is much weaker. All MACs obtained on the SAM surface are within a narrow range of 0.86 ± 0.05.

3.6. The mass effect on the TAC and MAC of a diatomic gas

3.6.1. The effect of the mass of gas molecules

We first tune the mass of N from 3.5 to 56 and calculate the TAC and MAC of the diatomic gas on a bare Au surface and a SAM surface. Accordingly, the gas–solid mass ratio varies from 0.036 to 0.57 on a bare Au surface and from 0.46 to 7.46 on a SAM surface. The MD simulation results are shown in Fig. 6(a) and (b). These results are similar to those of monoatomic gases shown in Fig. 2(e) and (f). On a bare Au surface, the TAC of a diatomic gas increases with gas–solid mass ratio, and the MAC is essentially a constant around 0.6.

When a bare Au surface is functionalized with SAMs, both the TAC and MAC are greatly enhanced. TACs on a SAM surface are around 0.8. No evident peak of the TAC on a SAM surface is observed in Fig. 6(a). This behavior can be related to the fact that the rotational motion of N_2 is more difficult to fully thermalize even with the SAM surface than translational motion as we discussed above. The MAC on a SAM surface is around 0.9 and essentially mass-ratio independent.

3.6.2. The effect of the mass of solid atoms

In this set of simulations, we fix the mass of N to 14 and tune the mass of the solid atom from 197 to 24.6. Accordingly, the gas–solid mass ratio varies from 0.142 to 1.14. The TAC and MAC of N_2 on a bare solid surface are shown in Fig. 6(c) and (d), respectively. These results are again very similar to those of monoatomic gases shown in Fig. 2(c) and (d). An evident decrease in the TAC occurs when there is a significant mass mismatch between the gas molecule and the solid atom. In Fig. 6(c), we also show the TAC of translational and rotational motions. It is seen that α_{tr} and α_T have similar mass-ratio dependence, while α_{rot} exhibits a monotonic increase with mass-ratio. The result indicates the rotational motions of N_2 are easier to thermalize on a surface with light solid atoms.

The MACs in Fig. 6(d) are all around 0.6. This result and all the previous results on the MAC show that a key factor that affects the MAC is the solid surface structure. The variation of the mass of gas molecules or solid atoms cannot change the structure or roughness of the surface. Hence, there is almost no mass effect on the MAC.

3.7. The effect of solid elasticity on the TAC and MAC of a diatomic gas

As we did in Section 3.4, the solid elasticity is tuned by varying the prefactor in the EAM potential from 0.3 to 5. It is seen in Fig. 7(a) that the TAC can be fitted by a linear function. However, the linear extrapolation of the TAC at $E = 0$ is not consistent with the TAC on a heavy-SAM surface. As we discussed in Section 3.4, the heavy-SAM surface mimics a bare Au surface with $E \to 0$. To understand the discrepancy, we show α_{tr} and α_{rot} in Fig. 7(a). It is seen both α_{tr} and α_{rot} have a good linear relationship with E if E is greater than 39 GPa. At $E = 23.4$ GPa, however, there is a sudden increase in α_{rot}. As we discussed in Section 3.4, such increase should be related to liquid-like surface structure at $E = 23.4$ GPa.

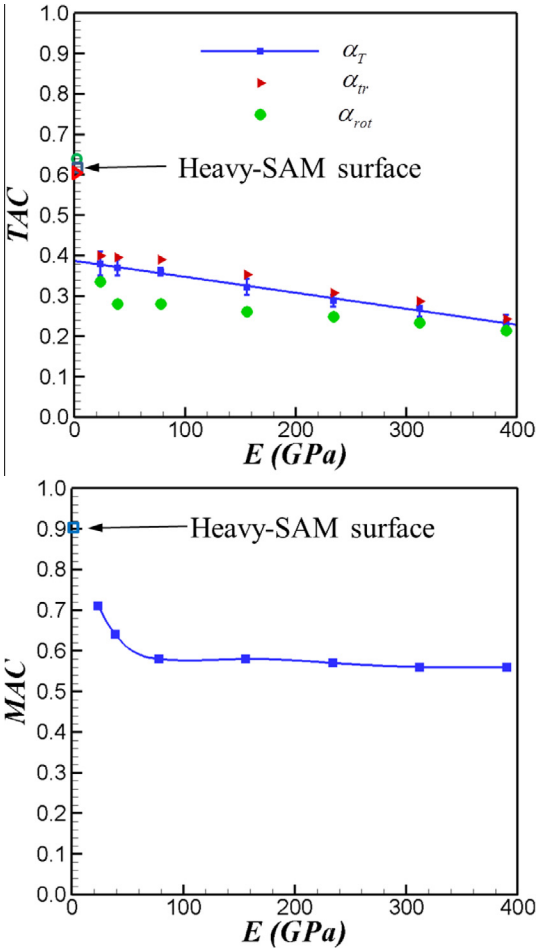

Fig. 7. The TAC and MAC of N_2 on a bare solid surface as a function of elastic modulus. (a) The TAC vs. elastic modulus. The open square, open triangle, and open circle symbols represent the TAC, the translational component of the TAC, and the rotational component of the TAC of N_2 on a heavy-SAM surface, respectively. (b) The MAC vs. elastic modulus. The open square symbol represents the MAC of N_2 on a heavy-SAM surface.

The results in Fig. 7(a) indicate α_{rot} is strongly affected by the solid surface structure. Using Eq. (7), we obtain $S^2(k)$ of a heavy-SAM surface at 300 K is about 0.16, which indicates a disordered surface structure. Moreover, the surface density of SAMs is 21.6 Å^2 per chain, which is only 1/3 of that of Au. A more sparse distribution of SAM molecules may also be responsible for much high TAC on the heavy-SAM surface. Similarly, the disordered surface structure also strongly affects the MAC of N_2. It is seen in Fig. 7(b) that the MAC exhibits a fast increase as the surface becomes disordered. On a heavy-SAM surface, the MAC of N_2 is about 0.9.

4. Summary and conclusions

The TAC and MAC of monoatomic and diatomic gases on a bare solid surface and a surface functionalized with SAMs are calculated through extensive MD simulations. The effects of the gas–solid mass ratio m_g/m_s, the solid–gas interaction strength ε_{sf}, the temperature T, and the solid elasticity E are studied. The following results are obtained.

(i) The TAC and MAC generally increase with the dimensionless quantity ε_{sf}/k_BT, which implies an increase of solid–gas interaction strength has about the same effect as a decrease

of temperature. The results are associated with the transition from collision type scattering to adsorption–desorption types of scattering.

(ii) On a bare solid surface, the TAC is independent on the gas–solid mass ratio if m_g/m_s is between 0.3 and 1.2. If m_g/m_s is out of this range, a large mass mismatch between gas and solid atoms leads to an evident decrease in the TAC.

(iii) On a SAM surface, the TAC of a monoatomic gas reaches a maximum when the gas atom has a perfect mass matching with the surface atom (sum of the three pseudo-atoms closest to the SAM surface). Such a maximum TAC is not observed for a diatomic gas on a SAM surface, which is due to rotational motions being more difficult to fully thermalize with a SAM surface.

(iv) The MAC is essentially independent of the gas–solid mass ratio. A key factor that affects the MAC is solid surface structure. The MAC is much higher on a disordered and rough surface than on an ordered smooth surface.

(v) As the solid modulus increases, the TAC decreases. A linear dependence of the TAC on elastic modulus E is found for an E of less than 390 GPa. As E gets close to 0, a nonlinear increase of α_{rot} with a decreasing E is observed. The fast increase in α_{rot} in the limit of $E \to 0$ is related to the liquid-like surface structure at a small E.

(vi) In all cases, the TAC and MAC on a SAM surface are significantly higher than those on a bare solid surface. A much softer and disordered SAM surface with improved gas–solid mass matching is responsible for the much higher TACs and MACs.

Most of our MD simulations were carried out at room temperatures or higher because these are the most relevant temperatures for the momentum and energy exchange between the solid and gas. At such temperatures classical statistics are suitable for gold (Debye temperature ~170 K [34]), and also good or reasonable for other metals. They are even more accurate for SAM layers characterized by softer vibrations. One can expect some effects of quantum mechanical statistics at much lower temperatures in case of metals, or even at room temperature for high Debye temperature materials, such as diamond (Debye temperature ~2200 K [35]). On the gas side classical statistics are very accurate for translational and rotational motions. Vibrations are expected to be frozen around room temperature, and thus accordingly we use rigid bond algorithm in our simulations to mimic this fact.

In this work, an atomistically smooth solid surface is used in the simulation. A real solid surface could be rough and contains defects, which leads to more diffuse scattering of gas molecules. The TAC and MAC on such surfaces will be greater than those at a smooth and perfect surface. Additionally, adsorbed layer could be formed on a contaminated surface. Previous studies [1,2] showed that gas energies are more easily to accommodate on surfaces with adsorbed layer. Hence, if the solid surface is not smooth and clean, the TAC and MAC could be greater than those predicted in this work.

Conflict of interest

None declared.

Acknowledgments

This work is supported by the U.S. Air Force Office of Scientific Research Grant No. FA9550-12-1-0351. We would like to thank the National Institute for Computational Science (NICS) for providing us supercomputer resources for MD simulations.

References

[1] Z. Liang, W. Evans, T. Desai, P. Keblinski, Improvement of heat transfer efficiency at solid–gas interfaces by self-assembled monolayers, Appl. Phys. Lett. 102 (2013) 061907.
[2] Z. Liang, W. Evans, P. Keblinski, Equilibrium and nonequilibrium molecular dynamics simulation of thermal conductance at solid–gas interfaces, Phys. Rev. E 87 (2013) 022119.
[3] S. Song, M.M. Yovanovich, F.O. Goodman, Thermal gap conductance of conforming surfaces in contact, J. Heat Transfer 115 (1993) 533.
[4] L. Biswal, S.K. Som, S. Chakraborty, Effects of entrance region transport processes on free convection slip flow in vertical microchannels with isothermally heated walls, Int. J. Heat Mass Transfer 50 (2007) 1248.
[5] K. Cao, A study of fundamental heat transfer behavior at near space altitudes, (Ph. D. dissertation), The University of Alabama, 2008.
[6] G.S. Springer, Heat Transfer in Rarefied Gases, Academic Press, New York, 1971. p. 164.
[7] J.C. Maxwell, On stresses in rarefied gases arising from inequalities of temperature, Phil. Trans. R. Soc. Lond. 170 (Pt. 1) (1879) 231.
[8] F.O. Goodman, H.Y. Wachman, Dynamics of Gas–Surface Scattering, Academic Press, New York, 1976. pp. 23–31.
[9] S.C. Saxena, R.K. Joshi, Thermal Accommodation and Adsorption Coefficients of Gases, Hemisphere Publishing Corporation, New York, 1989 (and references there in).
[10] B. Cao, M. Chen, Z. Guo, Temperature dependence of the tangential momentum accommodation coefficient for gases, Appl. Phys. Lett. 86 (2005) 091905.
[11] G.S. Hwang, M. Kaviany, Molecular dynamics simulation of effective thermal conductivity of vapor filled nanogap and nanocavity, J. Appl. Phys. 106 (2009) 024317.
[12] L. Hu, A.J.H. McGaughey, Energy accommodation between noble gases carbon nanotubes, J. Phys. Chem. C 117 (2013) 18804.
[13] S.A. Schaaf, P.L. Chambre, Flow of rarefied gases, in: H.W. Emmons (Ed.), Fundamentals of Gas Dynamics, vol. III, Princeton Univ. Press, Princeton, NJ, 1958, p. 687.
[14] S.M. Foiles, M.I. Baskes, M.S. Daw, Embedded-atom-method functions for the fcc metals Cu, Ag, Au, Ni, Pd, Pt and their alloys, Phys. Rev. B 33 (1986) 7983.
[15] G.C. Maitland, M. Rigby, E.B. Smith, W.A. Wakeham, Intermolecular Forces: Their Origin and Determination, Clarendon Press, Oxford, 1981.
[16] V.R. Cervellera, M. Alberti, F. Huarte-Larranaga, A molecular dynamics simulation of air adsorption in single-walled carbon nanotube bundles, Int. J. Quant. Chem. 108 (2008) 1714.
[17] P.S. Cheung, J.G. Powles, The properties of liquid nitrogen. IV. A computer simulation, Mol. Phys. 30 (1975) 921–949.
[18] J. Hautman, M.L. Klein, Simulation of monolayer of alkyl thiol chains, J. Chem. Phys. 91 (1989) 4994.
[19] A. Koike, M. Yoneya, Chain length effects on frictional behavior of confined ultrathin films of linear alkanes under shear, J. Phys. Chem. B 102 (1998) 3669.
[20] R. Mahaffy, R. Bhatia, B.J. Garrison, Diffusion of a butanethiolate molecule on a Au{1 1 1} surface, J. Phys. Chem. B 101 (1997) 771.
[21] A.K. Rappe, C.J. Casewit, K.S. Colwell, W.A. Goddard, W.M. Skiff, UFF, a full periodic table force field for molecular mechanics and molecular dynamics simulations, J. Am. Chem. Soc. 114 (1992) 10024.
[22] D. Frenkel, B. Smit, Understanding Molecular Simulation, Springer, Berlin, 2002. p. 75, p. 426..
[23] I.P. Omelyan, Algorithm for numerical integration of the rigid-body equations of motion, Phys. Rev. E 58 (1998) 1169.
[24] H.J.C. Berendsen, J.P.M. Postma, W.F. Van Gunsteren, A. Di Nola, J.R. Haak, Molecular dynamics with coupling to an external bath, J. Chem. Phys. 81 (1984) 3684.
[25] P. Jund, R. Jullien, Molecular-dynamics calculation of the thermal conductivity of vitreous silica, Phys. Rev. B 59 (1999) 13707.
[26] B.S. Day, J.R. Morris, Packing density and structure effects on energy transfer dynamics in argon collisions with organic monolayers, J. Chem. Phys. 122 (2005) 234714.
[27] S.R. Cohen, R. Naaman, J. Sagiv, Translational energy transfer from molecules and atoms to adsorbed organic monolayers of long-chain amphiphiles, Phys. Rev. Lett. 58 (1987) 1208.
[28] N. Isa, K.D. Gibson, T. Yan, W. Hase, S.J. Sibener, Experimental and simulation study of neon collision dynamics with a 1-decanethiol monolayer, J. Chem. Phys. 120 (2004) 2417.
[29] E.H. Kennard, Kinetic Theory of Gases, McGraw-Hill Book Company Inc, New York and London, 1938. pp. 100–105.
[30] S. Borisov, S. Litvinenko, Y. Semenov, P. Suetin, Experimental investigation of the temperature dependence of the accommodation coefficients for the gases He, Ne, Ar, and Xe on a Pt surface, J. Eng. Phys. Thermophys. 34 (1978) 603.
[31] G. Simons, H. Wang, Single Crystal Elastic Constants and Calculated Aggregate Properties, MIT Press, Cambridge, MA, 1977.
[32] S.R. Phillpot, J.F. Lutsko, D. Wolf, S. Yip, Molecular dynamics study of lattice-defect-nucleated melting in silicon, Phys. Rev. B 40 (1989) 2831–2840.
[33] B.J. Lee, J.H. Shim, M.I. Baskes, Semiempirical atomic potentials for the fcc metals Cu, Ag, Au, Ni, Pd, Pt, Al, and Pb based on first and second nearest-neighbor modified embedded atom method, Phys. Rev. B 68 (2003) 144112.
[34] C. Kittel, Introduction to Solid State Physics, eighth ed., John Wiley & Sons, USA, 2004.
[35] K.A. Gschneidner, Jr, in: F. Seitz, D. Turnbull (Eds.), Solid State Physics, vol. 16, Academic Press, New York, 1964, pp. 275–426.